Available online at www.sciencedirect.com
SCIENCE DIRECT®
Journal of Non-Crystalline Solids 347 (2004) 144–152
JOURNAL OF NON-CRYSTALLINE SOLIDS
www.elsevier.com/locate/jnoncrysol

UV-laser-induced densification of fused silica: a molecular dynamics study

Lianqing Zheng [a,b,*], John C. Lambropoulos [a,b,*], Ansgar W. Schmid [b]

[a] Department of Mechanical Engineering, University of Rochester, Rochester, NY 14627, USA
[b] Laboratory for Laser Energetics, University of Rochester, 250 E. River Road, Rochester, NY 14623-1299, USA

Received 19 May 2004; received in revised form 24 June 2004
Available online 29 September 2004

Abstract

Classical molecular dynamics simulations have been performed to study the UV-laser-induced densification in fused silica. Relationships between induced densification and absorbed laser fluence under different laser durations are established. We have also studied the effects of laser irradiation on the radial distribution functions, static structure factor, bond-angle distributions, ring-size distribution, and elastic constants of fused silica. While the Si–O bond length is little affected by laser irradiation, the lengths of O–O and Si–Si and bond-angle distributions of ∠Si–O–Si and ∠O–Si–O are undergoing larger changes. The number of dominant 6-member rings decreases after laser irradiation, and that of rings of other sizes increases. Young's modulus, bulk modulus, and Lamé constant of fused silica increase rapidly with increasing density.

PACS: 31.15.Qg; 61.43.Fs; 61.80.Ba

1. Introduction

With the development of optical lithography in semiconductor fabrication, deep-UV-lasers (248 nm and 193 nm) are widely used to achieve finer resolution. As a choice and leading optical material in illumination and projection systems in microlithography, high-purity fused silica (amorphous silicon dioxide, a-SiO_2) exhibits many excellent optical, mechanical, physical, and chemical properties, such as high transmittance at UV wavelength, very low thermal expansion coefficient, high degree of homogeneity, ease of fabrication into lenses, chemical stability, etc. [1,2].

As early as 1953, vitreous silica was observed to compact permanently under fast neutron irradiation and its refractive index was found to increase [3]. Densification induced by γ rays, electrons, protons, and deuterons was also observed [4]. In 1986, for the first time, Fiori and Devine studied 248 nm laser-induced changes in a-SiO_2 thin films with a laser fluence of 300 mJ/cm^2 [5]. Since then, intensive experimental efforts have been undertaken to study UV-laser-induced densification of bulk fused silica [1,6–11]. Though several empirical relationships between induced densification and applied laser doses have been proposed and have similar forms, the mechanism of UV-laser-induced densification in fused silica still remains unclear and poorly understood.

Molecular dynamics (MD) has proved to be a powerful tool for studying both microscopic and macroscopic properties of materials. Many studies have been dedicated to understanding the microstructural properties [12–15] and pressure-induced densification [16–18] of fused silica. Less attention has been focused, however,

* Corresponding authors. Tel.: +1 585 275 5927; fax: +1 585 275 5960 (L. Zheng), tel.: +1 585 275 4070; fax: +1 585 256 2509 (J.C. Lambropoulos).
E-mail addresses: lzheng@me.rochester.edu (L. Zheng), jcl@me.rochester.edu (J.C. Lambropoulos).

0022-3093/$ - see front matter © 2004 Published by Elsevier B.V.
doi:10.1016/j.jnoncrysol.2004.07.062

on how UV-laser irradiation causes densification in fused silica and how laser irradiation affects its properties. Kubota et al. [19] used shock waves to model laser pulses to achieve densification of up to 20% in fused silica. Wootton and his colleagues [20] modeled the laser absorption process in fused silica as added kinetic energy in excited Si–O bonds and also produced densification. They proposed that the radiation-induced compaction could be regarded as a localized melting immediately followed by a rapid quench [20].

In the present study, we use classical molecular dynamics to study UV-laser-induced densification in fused silica. The model of laser irradiation is similar to the method in Ref. [20]. The relationship between induced densification and absorbed laser fluence is investigated for different laser pulse durations. We also perform detailed studies on the effects of laser irradiation on the microstructures (radial distribution functions, static structure factor, bond-angle distributions, and ring-size distribution) and elastic properties of fused silica.

2. Computational techniques

2.1. Equations of motion

Given N atoms in a triclinic simulation cell, we denote the edge vectors of the cell as $\vec{a},\vec{b},\vec{c}$, respectively. To avoid cell rotating during simulation, we restrict the components of these vectors with $a_y = a_z = b_z = 0$, $a_x > 0$, $b_y > 0$, and $c_z > 0$ [21]. The coordinates of atom i are denoted as $\vec{r}_i$ and its corresponding coordinates in reciprocal space $\vec{s}_i$ are equal to $\mathbf{H}^{-1}\vec{r}_i$, where the matrix $\mathbf{H}$ is defined as

$$\mathbf{H} = \{\vec{a},\vec{b},\vec{c}\} = \begin{bmatrix} a_x & b_x & c_x \\ 0 & b_y & c_y \\ 0 & 0 & c_z \end{bmatrix}. \tag{1}$$

To achieve an isothermal–isotension ($N\mathbf{t}T$) ensemble, the following Lagrangian is constructed [22–25]:

$$\begin{aligned}\mathscr{L}(\vec{s}_i,\dot{\vec{s}}_i,\mathbf{H},\dot{\mathbf{H}},\zeta,\dot{\zeta}) = {} & \frac{1}{2}\sum_{i=1}^{N} m_i\zeta^2\dot{\vec{s}}_i^{\mathrm{T}}\mathbf{G}\dot{\vec{s}}_i - U^{\mathrm{tot}} \\ & + \frac{1}{2}M_P\zeta^2\mathrm{Tr}(\dot{\mathbf{H}}^{\mathrm{T}}\dot{\mathbf{H}}) - p_{\mathrm{ext}}V \\ & - V_0\mathrm{Tr}(\mathbf{t}\epsilon) + \frac{1}{2}M_T\dot{\zeta}^2 \\ & - gk_{\mathrm{B}}T_{\mathrm{ext}}\ln(\zeta),\end{aligned} \tag{2}$$

where ζ is the time-scale variable for temperature coupling; m_i is the mass of atom i; $\boldsymbol{G} = \boldsymbol{H}^{\mathrm{T}}\boldsymbol{H}$; U^{tot} is the total potential energy of the simulation cell; M_P and M_T are the mass parameters for stress and temperature coupling, respectively; p_{ext} is the external hydrostatic pressure and T_{ext} the external temperature; V is the volume of the simulation cell; $\mathbf{t}$ is the thermodynamical tension [23] and the strain matrix $\epsilon = \frac{1}{2}(\mathbf{H}_0^{-1\mathrm{T}}\mathbf{G}\mathbf{H}_0^{-1} - 1)$; k_{B} is the Boltzmann's constant and g is the degrees of freedom; subscript '0' denotes the values at zero stress, superscript 'T' the transpose of a matrix or vector, and 'Tr' the trace of a matrix. The time derivative is with respect to the scaled time t, which is related to the real time t' by

$$\mathrm{d}t' = \frac{\mathrm{d}t}{\zeta}. \tag{3}$$

The equations of motion are then derived from the above Lagrangian with the assumption that the potential energy has only two-body terms:

$$\ddot{\vec{s}}_i = -\frac{\mathbf{H}^{-1}}{m_i}\sum_{j\neq i}\frac{\partial U(r_{ij})}{\partial r_{ij}}\frac{\vec{r}_{ij}}{r_{ij}} - \left(\mathbf{G}^{-1}\dot{\mathbf{G}} + \frac{\dot{\zeta}}{\zeta}\mathbf{I}\right)\dot{\vec{s}}_i, \tag{4a}$$

$$M_P\ddot{\mathbf{H}} = -M_P\frac{\dot{\zeta}\dot{\mathbf{H}}}{\zeta} + (\mathbf{P} - p_{\mathrm{ext}}\mathbf{I})V\mathbf{H}^{-1T} - \mathbf{H}\Gamma, \tag{4b}$$

$$\ddot{\zeta} = \frac{\dot{\zeta}^2}{\zeta} + \frac{\zeta}{M_T}\left[\sum_{i=1}^{N} m_i\dot{\vec{r}}_i^{\mathrm{T}}\dot{\vec{r}}_i + M_P\mathrm{Tr}(\dot{\mathbf{H}}^{\mathrm{T}}\dot{\mathbf{H}}) - gk_{\mathrm{B}}T_{\mathrm{ext}}\right], \tag{4c}$$

where $\vec{r}_{ij} = \vec{r}_i - \vec{r}_j$ and $r_{ij} = |\vec{r}_{ij}|$, $\mathbf{P}$ is the pressure tensor, $\mathbf{I}$ is the identity matrix, $\Gamma = V_0\mathbf{H}_0^{-1}\mathbf{t}\mathbf{H}_0^{-1\mathrm{T}}$, and time derivatives are with respect to the real time.

If we fix $\mathbf{H}$, i.e., $\dot{\mathbf{H}} = 0$, we have equations for constant volume and constant temperature (NVT) ensemble. If both $\mathbf{H}$ and ζ are fixed, then Eqs. (4a)–(4c) will produce a constant volume and constant energy (NVE) ensemble.

2.2. Potential energy for SiO_2

In this study, we use a modified BKS potential for silica [26,27], which includes a Coulomb term, a Buckingham potential, and a 30-6 LJ potential:

$$\begin{aligned}U(r_{ij}) = {} & k_{\mathrm{C}}\frac{q_iq_j}{r_{ij}} + A_{ij}\mathrm{e}^{-b_{ij}r_{ij}} - \frac{C_{ij}}{r_{ij}^6} \\ & + 4\epsilon_{ij}\left[\left(\frac{\sigma_{ij}}{r_{ij}}\right)^{30} - \left(\frac{\sigma_{ij}}{r_{ij}}\right)^{6}\right],\end{aligned} \tag{5}$$

where k_{C} is the Coulomb constant, atomic charge of Si $q_{\mathrm{Si}} = +2.4\mathrm{e}$, and atomic charge of O $q_{\mathrm{O}} = -1.2\mathrm{e}$; the other parameters are listed in Table 1.

The Coulomb term in BKS potential is calculated by the smooth particle mesh Ewald method (SPME) [28]. The linked-list method [29] is used to compute the short-range terms (direct space part in Ewald sum for Coulomb term, Buckingham potential, and LJ potential) with a cutoff distance of 1.0 nm. Long-range corrections

Table 1
Atomic parameters in modified BKS potential

	A_{ij}[a] (kJ mol^{-1})	b_{ij}[a] (nm)	c_{ij}[a] (kJ mol^{-1} nm^6)	ϵ_{ij}[b] (kJ mol^{-1})	σ_{ij}[b] (nm)
SiO	1 737 098.6612	48.7318	0.01288447	0.2989065	0.1313635
OO	133 996.2371	27.6000	0.01688494	0.1014110	0.1779239
SiSi	0.0	0.0	0.0	0.0	0.0

[a] Ref. [26].
[b] Ref. [27].

for the total potential energy and pressure tensor due to cutoff in short-range potentials are also calculated [30].

2.3. Simulation of laser irradiation

The effect of laser irradiation is modeled by the energy transfer from the absorbed laser photons to the bonded silicon and oxygen atoms [20,31]. We assume that the energy of absorbed laser photons is converted into the kinetic energy of a pair of bonded Si and O atoms. Absorbing Si–O bonds are selected randomly, and then new velocities are assigned to the atoms in each selected bond, assuming that the total kinetic energy change is equal to the absorbed photon energy and the total momentum remains the same as before absorption, i.e.,

$$\frac{1}{2}m_{\mathrm{Si}}\vec{v}_{\mathrm{Si}}^{\,2}+\frac{1}{2}m_{\mathrm{O}}\vec{v}_{\mathrm{O}}^{\,2}=E^{0}_{k,\mathrm{SiO}}+\Delta E \tag{6}$$

and

$$m_{\mathrm{Si}}\vec{v}_{\mathrm{Si}}+m_{\mathrm{O}}\vec{v}_{\mathrm{O}}=\vec{p}^{\,0}_{\mathrm{SiO}}, \tag{7}$$

where m_{Si}, m_{O} are the atomic masses; $\vec{v}_{\mathrm{Si}}, \vec{v}_{\mathrm{O}}$ are the velocities of Si and O atoms in the selected bond after photon absorption, respectively; $E^{0}_{k,\mathrm{SiO}}$ is the total kinetic energy of these two atoms before absorption; ΔE is the energy of absorbed photons; and $\vec{p}^{\,0}_{\mathrm{SiO}}$ is the total linear momentum of the bond before absorption. Note that there are six unknowns ($\vec{v}_{\mathrm{Si}}$ and $\vec{v}_{\mathrm{O}}$) but only four equations, so two unknowns must be determined randomly, say v^{x}_{Si} and v^{y}_{Si}. Then it is trivial to solve for the rest of the unknowns from Eqs. (6) and (7). To ensure that all the roots are real, the randomly assigned velocities v^{x}_{Si} and v^{y}_{Si} have to satisfy the following relation:

$$\left(v^{x}_{\mathrm{Si}}-\frac{p^{0x}_{\mathrm{SiO}}}{m_{\mathrm{Si}}+m_{\mathrm{O}}}\right)^{2}+\left(v^{y}_{\mathrm{Si}}-\frac{p^{0y}_{\mathrm{SiO}}}{m_{\mathrm{Si}}+m_{\mathrm{O}}}\right)^{2} < \frac{m_{\mathrm{O}}}{m_{\mathrm{Si}}(m_{\mathrm{Si}}+m_{\mathrm{O}})}\left[2\left(E^{0}_{\mathrm{SiO}}+\Delta E\right)-\frac{|\vec{p}^{\,0}_{\mathrm{SiO}}|^{2}}{m_{\mathrm{Si}}+m_{\mathrm{O}}}\right]. \tag{8}$$

3. Simulation procedure

The initial configuration of the simulation cell is obtained from an algorithm developed by Vink and Barkema [32]. Unlike the melting/cooling method of glass-making, this algorithm directly generates a continuous random network (CRN) of silica glass by the so-called bond transpositions [33]. Some advantages of this method over the melting/cooling process are (1) better agreement with the experimental value for density, (2) smaller bond-angle variations, and (3) the near absence of coordination defects.

In this study, we use a cubic simulation cell containing 1506 atoms (502 Si atoms and 1004 O atoms) with an initial density of 2.20 g/cm^3. Periodic boundary conditions are applied in all three directions. Equations of motion are solved by a modified Beeman integrator [21] with a time step of 1 fs. We first equilibrate the cell at 300 K and zero stress for 300 ps under $N\mathbf{t}T$ ensemble. The initial velocities are generated with a Maxwell distribution [30]. After relaxation, the cell shrinks a little and the density increases to 2.30 g/cm^3, which is still in good agreement with the experimental value of 2.20 g/cm^3. Laser irradiation is then applied to the cell (also under $N\mathbf{t}T$ ensemble) with a constant interval between two adjacent absorptions for one simulation. This interval of laser photon absorption varies from 500 to 8 time steps to simulate different laser fluences for a given laser pulse duration. During the simulations, we typically consider up to 6250 photon absorptions (equivalent to an absorbed fluence of approximately 0.16 J/cm^2). After irradiation, the cell is allowed at least 200 ps to reach equilibrium again. The ensemble is then switched to NVE for 1 ns to collect the properties of the simulation cell.

Densification of a cell after laser irradiation is defined by

$$D=\frac{\rho_{\mathrm{d}}-\rho_0}{\rho_0}=\frac{V_0}{V_{\mathrm{d}}}-1, \tag{9}$$

where ρ_0, ρ_{d}, V_0, and V_{d} are the densities and volumes of the simulation cell before and after irradiation, respectively. The *absorbed* laser fluence F_{l} is calculated by

$$F_{\mathrm{l}}=\frac{N_{\mathrm{ph}}hc}{\lambda V_0^{2/3}}, \tag{10}$$

where N_{ph} is the number of absorbed photons, λ is the laser wavelength, h is the Planck's constant, and c is the velocity of light in vacuum. In the present study, we use, λ = 193 nm and exclusively two-photon absorp-

tion [7,20], i.e., ΔE in Eq. (6) is 12.8 eV for each absorption.

4. Results

4.1. UV-laser-induced densification

To have reasonable statistical results, 12 simulation cells with the same initial atomic configuration but different initial velocities are used, and for each laser fluence, at least 20 independent simulations are performed. Fig. 1 shows a typical evolution of temperature, total potential energy (U^{tot}), and cell volume with simulation time. In the case presented in Fig. 1, the interval of absorption is 25 time steps and the irradiation duration (τ) is 50 ps.

Two sets of simulations with different laser irradiation durations ($\tau = 50$ ps and $\tau = 100$ ps, respectively) have been carried out. Fig. 2 presents the results of induced densification versus absorbed laser fluence. For $\tau = 50$ ps, densification increases with laser fluence until

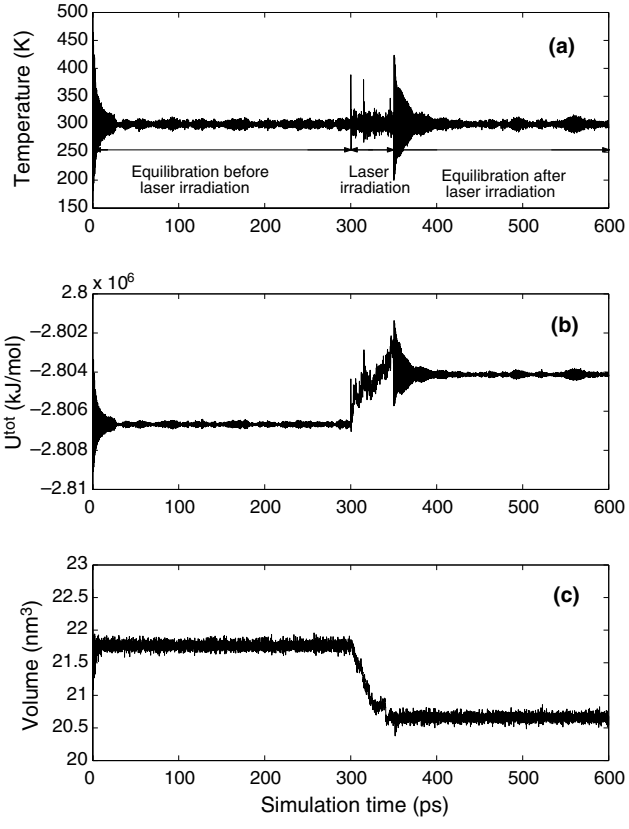

Fig. 1. Typical evolution of (a) temperature, (b) total potential energy, and (c) cell volume with simulation time. In this case, the interval of photon absorption is 25 time steps, and the total number of absorptions is 2000. The simulation cell is equilibrated at 300 K and zero stress for 300 ps, irradiated for 50 ps, and then allowed 250 ps to reach equilibrium again.

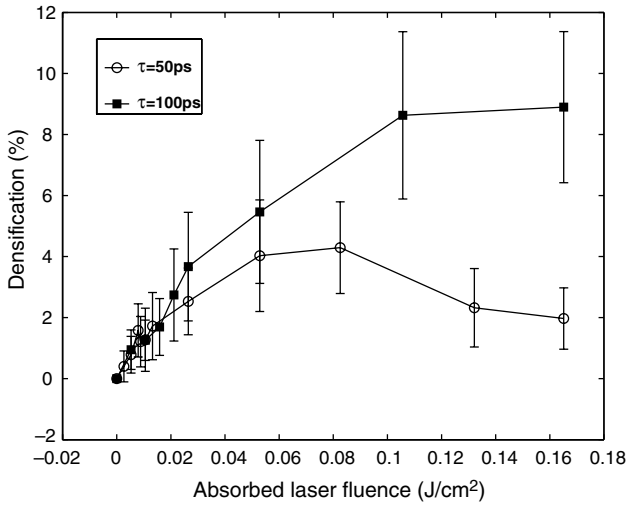

Fig. 2. MD simulation results of UV-laser-induced densification in fused silica versus absorbed laser fluence for $\tau = 50$ ps and $\tau = 100$ ps, respectively. At least 20 independent simulations were performed for each fluence in each laser duration, and the error bars represent the corresponding standard deviations. When absorbed laser fluence is small (<0.02 J/cm^2), $D = 128.74\ F_l$ regardless of laser pulse duration.

it reaches its maximum at $F_l = 0.08$ J/cm^2; then densification decreases. In the case of $\tau = 100$ ps, though laser-induced densification increases monotonically within the studied fluences, it gradually reaches a plateau after $F_l = 0.11$ J/cm^2. It is interesting to note that both intervals of absorption at the maximum densifications are 16 time steps. This might indicate a threshold of laser intensity (F_l/τ, or the interval of absorption in MD simulation) above which part of fused silica would tend to expand against compaction. Curves in Fig. 2 become independent of duration τ for F_l less than 0.02 J/cm^2, and densification is then linearly related to fluence by

$$D = 128.74F_l, \text{ for } F_l < 0.02 \text{ J/cm}^2, \tag{11}$$

where D is in percentage and F_l in J/cm^2, and the coefficient is obtained through a least-squares fit of data for both $\tau = 50$ ps and $\tau = 100$ ps. When F_l is above 0.02 J/cm^2, densification with $\tau = 100$ ps is larger than with $\tau = 50$ ps at the same laser fluence. This is probably because the cell with longer time between two absorptions could adjust itself more to form a denser structure. While this argument is apparently not true in the case of very large τ, where densification would be small since laser irradiation has little effect on fused silica, a threshold of τ at which densification reaches a maximum under a certain fluence would be of interest for further study.

We have compared our results and previous studies, including both MD simulations and experiments. In Wootton *et al.*'s study [20], a simulation cell containing 864 atoms was used, and temperature and pressure were fixed at 300 K and 1 atm by Gaussian constraints, respectively. Their interval of excitations was 1000 time

steps (each time step was 1.018 fs), and the number of excitations was up to 200. Their amorphous silica configurations were obtained by cooling melted β-quartz and had an initial density of 2.56 g/cm^3 (from a cooling rate of 10^{12} K/s). An excitation energy of 10 eV was used in their simulation of laser irradiation. We have estimated the absorbed laser fluence in their simulation according to Eq. (10) with $\rho_0 = 2.56\,\mathrm{g/cm^3}$, $V_0 = 11.22\,\mathrm{nm^3}$, and $\lambda = 248\,\mathrm{nm}$. Their maximum F_l was about 0.0064 J/cm^2. Densification at this fluence is about 0.82% according to Eq. (11) in our study, while it was about 5.5% from their results. The discrepancy is not surprising because of different initial configurations of fused silica and laser excitation energy. They also found a linear relationship between densification and fluence for low fluences.

An empirical formula has been experimentally established to describe the relation of UV-laser-induced densification in fused silica and applied laser doses and has the following form [1,8,9]:

$$\delta = a\left(N_p \frac{I^2}{\tau}\right)^b, \tag{12}$$

where δ is the densification in ppm, N_p is the number of laser pulses in millions, I is the *incident* laser fluence per pulse in mJ/cm^2, a and b are coefficients determined empirically, and the units of laser pulse duration τ are in ns. Coefficients a and b vary with different experimental conditions and grades of silica glass, but b falls in the range of 0.5–0.7. If we take $a = 0.30$ and $b = 0.7$ [9] and consider an absorption rate of 0.5% for fused silica at 193 nm [34], we estimate a densification of 5.4 ppm according to Eq. (12) for one of our MD simulation conditions: $F_l = 0.0088\,\mathrm{J/cm^2}$, $\tau = 0.05\,\mathrm{ns}$, and $N_p = 10^{-6}$ million. This is three orders of magnitude smaller than the MD simulated densification (1.2%). For the largest fluence in our simulation, Eq. (12) predicts a densification of 326.8 ppm for $\tau = 0.05$ ns, which is still two orders of magnitude smaller than the simulation result (2.0%). This discrepancy is probably due to the large differences in irradiation conditions. A typical fluence of a UV-laser in densification experiment is of the order of 10 mJ/cm^2 (equivalent to an absorbed fluence of 0.05 mJ/cm^2 in MD simulation), and pulse duration is about 20 ns. It is very likely that Eq. (12) found in these experimental conditions is no longer satisfied under MD simulation conditions. Fig. 2 also indicates that a different functional form of D versus F_l relation may exist for different laser pulse durations. On the other hand, our densification results are comparable to those from higher-laser-fluence experiments. Fiori and Devine [5] used a 248 nm laser with a fluence of 300 mJ/cm^2 and a pulse duration of 20 ns to study the densification of a-SiO_2 thin film. For an accumulated dose of 30 J/cm^2 (equivalent to an absorbed fluence of 0.16 J/cm^2), a densification of approximately 1% was achieved. A 10 μm-thick layer of 20% densification has also been found on a fused silica surface in a high-fluence, 355 nm laser damage test [35].

4.2. Effects of laser irradiation on the properties of fused silica

To investigate how UV-laser irradiation affects the properties of fused silica, we have studied its microstructural and elastic properties before and after irradiation. For convenience, we name Cell#l an unirradiated cell, Cell#2 a cell irradiated by a laser pulse of $F_l = 0.053$ J/cm^2 and $\tau = 50$ ps and producing a densification of 8.4%, and Cell#3 a cell irradiated by a laser pulse of $F_l = 0.106$ J/cm^2 and $\tau = 100$ ps and producing a densification of 14.8%.

The radial distribution functions (RDFs) $g_{\alpha\beta}(r)$ are presented in Fig. 3. The magnitudes of the first peaks in the RDFs are found to decrease with increasing density. While the position of $g_{SiO}(r)$'s first peak does not change, those of $g_{OO}(r)$ and $g_{SiSi}(r)$ decrease slightly. The second peak of $g_{SiSi}(r)$ changes much more significantly than those of the other two: it becomes flatter and moves toward smaller distance. We have also studied the change of coordination numbers of Si and O atoms and present the results in Table 2. The coordination number of an atom is defined as the number of its nearest neighbors, while the cutoff distance for the nearest neighbors is the position of the minimum between the first and second peaks in corresponding RDF. For unirradiated fused silica, each Si atom is connected with four O atoms and each O atom with two Si atoms. Upon irradiation, both under-coordinated and over-coordinated defects are found. The number of over-coordi-

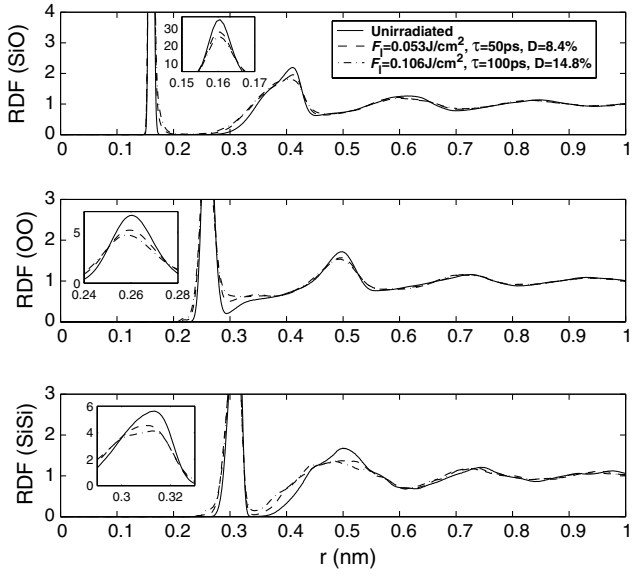

Fig. 3. Radial distribution functions of fused silica before and after UV-laser irradiation. The insets are the enlargements of the first peaks.

Table 2
Change of the coordination numbers after laser irradiation

Coordination number	Cell#1		Cell#2		Cell#3	
	Si (%)	O (%)	Si (%)	O (%)	Si (%)	O (%)
1				0.7		0.1
2		100		98.2		96.0
3			0.6	1.1		3.9
4	100		98.0		92.4	
5			1.4		7.6	

nated atoms increases with induced densification, i.e., each atom tends to have more neighbors and macroscopically the material becomes denser.

From RDFs, one can calculate the neutron-scattering static structure factor $S_N(q)$ [36]. In Fig. 4 we compare $S_N(q)$ of Cell#1, Cell#2, and Cell#3, along with an experimental result for a fused silica sample with a density of 2.32 g/cm^3 [37]. The first sharp peak in $S_N(q)$ moves toward higher q (from 15.6 nm^{-1} to 16.5 nm^{-1} to 17.2 nm^{-1}) and decreases in magnitude with increasing density, while the second peak shifts toward lower q (from 30.3 nm^{-1} to 29.7 nm^{-1} to 29.6 nm^{-1}). Changes in the third and further peaks are relatively small, indicating the change of the short-range order in fused silica is small. Similar observations were reported in experimental studies on pressure-induced densification of silica glass [37,38].

The bond-angle distributions (BAD) are shown in Fig. 5. In the ∠O–Si–O BAD, one sharp peak is centered at 109.39° for the unirradiated fused silica cell; this peak moves toward lower angle and its magnitude decreases after laser irradiation. In the ∠Si–O–Si BAD, a broad peak is centered at 145.68° in the unirradiated state; similarly, its magnitude decreases with density and position moves toward lower angle. A small peak

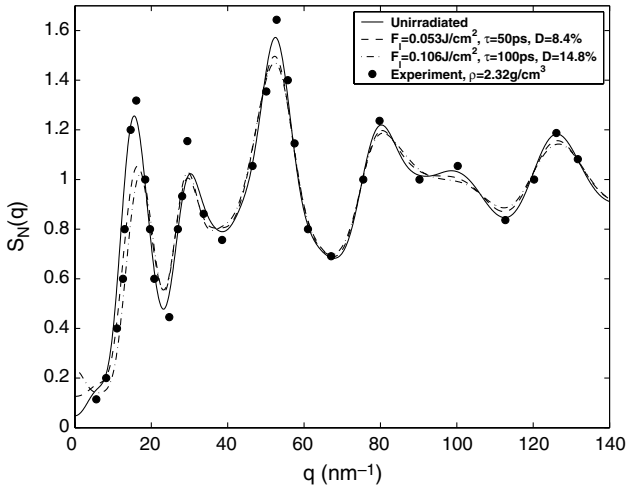

Fig. 4. Comparison of the neutron scattering static structure factors $S_N(q)$. The experimental data are taken from Ref. [37].

at about 100° is found in Cell#3. In the ∠Si–Si–Si BAD, the peak is broad with a flat top, and the mean value of ∠Si–Si–Si shifts from 108.61° (Cell#1) to 106.98° (Cell#2) to 106.19° (Cell#3); the flat top broadens with density and a small peak around 60° appears in Cell#2 and Cell#3. There are two peaks in the ∠Si–Si–O BAD: one at 25.93° and the other at 106.63° in the unirradiated cell. With increasing density, the first peak moves toward higher angle (18.83° in Cell#2 and 19.93° in Cell#3) and the second peak moves in the opposite direction (104.48° in Cell#2 and 102.23° in Cell#3). In the ∠Si–O–O BAD for Cell#l, one sharp peak is found at 35.58°, followed by a broad band tail from 80° to 180°. This sharp peak moves slightly toward higher angle after irradiation, and the broad band becomes even broader, ranging from about 55° to 180°. Similarly, a sharp peak is followed by a very blunt peak in the ∠O–O–O BAD. While this sharp peak at 59.48° is barely affected by laser irradiation, the blunt peak at about 135° increases greatly in magnitude and moves toward lower angle with increasing density induced by irradiation.

The ring structure in amorphous silica is a well-accepted concept [39]. A ring is defined as a closed path consisting of Si–O bonds. The number of Si atoms in a ring is used to represent the size of this ring, i.e., an n-member ring contains n Si atoms and $2n$ Si–O bonds. The ring-size distribution is a statistical distribution of the number of rings around a given Si atom. Here we are interested only in primitive rings that cannot be decomposed into two or more smaller rings [40]. An efficient algorithm is used to collect this property [40]. Simulation results for the ring-size distribution of up to 10-member rings are presented in Fig. 6. In the unirradiated state, the ring-size distribution peaks at the 6-member ring, and there are no rings of size smaller than 4 found in Cell#l, which indicates an excellent thermal equilibrium in the cell [41]. After irradiation, the number of 6-member rings decreases and that of rings of other sizes increases. The appearance of 3-member rings contributes to the peak at 60° in the ∠Si–Si–Si BAD of the densified cells, while the peak at 100° in the ∠Si–O–Si BAD of Cell#3 is due to 2-member rings. With a densification of 14.8%, the dominant ring size changes from 6 to both 6 and 7. Another MD study reports similar results for a shock wave densified fused silica cell [19].

According to above observations on the changes of the microstructural properties of fused silica upon laser irradiation, the absorbed photon energy activates the reconstruction of silica structures, and Si atoms are brought closer to their Si neighbors and so are O atoms to their O neighbors. This eventually forms a denser phase of fused silica under the same temperature and pressure.

We also investigate the change of elastic properties of fused silica after laser irradiation. The adiabatic elastic

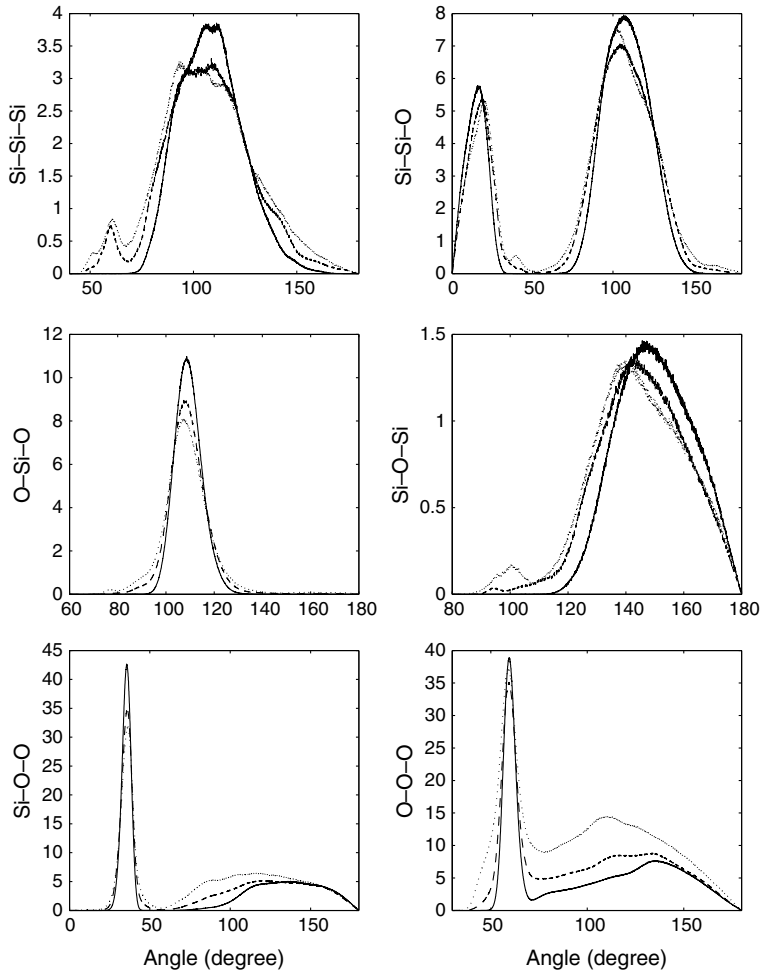

Fig. 5. Bond-angle distributions of fused silica before and after UV-laser irradiation. Solid lines represent unirradiated Cell#l, dashed lines Cell#2, and dotted lines Cell#3.

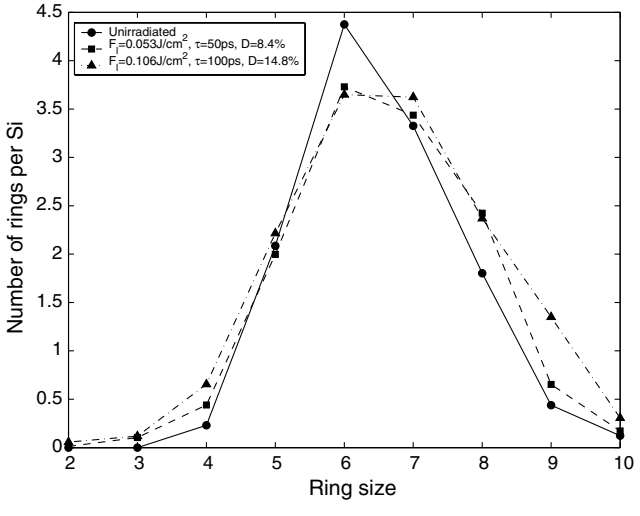

Fig. 6. Ring-size distributions of fused silica before and after UV-laser irradiation.

constants are calculated in *NVE* ensemble under zero stress by [42]

$$C_{ijkl} = -\frac{V}{k_B T}\delta(P_{ij}, P_{kl}) + \frac{2Nk_B T}{V}(\delta_{il}\delta_{jk} + \delta_{ik}\delta_{jl}) + \frac{1}{V}\left\langle \sum_{a=1}^{N}\sum_{b>a}^{N} f(r_{ab}) r_{ab}^{i} r_{ab}^{j} r_{ab}^{k} r_{ab}^{l} \right\rangle, \quad (13)$$

where fluctuations $\delta(P_{ij}, P_{kl}) = \langle P_{ij}P_{kl}\rangle - \langle P_{ij}\rangle\langle P_{kl}\rangle$, P_{ij} is the pressure tensor, T is the temperature of the simulation cell, r_{ab}^{i} is the ith component of vector $\vec{r}_{ab}$, angular brackets denote ensemble average, and function $f(r) = [U''(r) - U'(r)/r]/r^2$. The instant parts in the first and third terms on the right-hand side of Eq. (13) are calculated every two time steps, and averages are taken every 100 ps in a simulation run of 1 ns. Table 3 lists the results for Young's modulus (E) bulk modulus (K), shear modulus (G), and Lamé constant (L) of fused silica. G is the average of C_{44}, C_{55}, and C_{66}; L is the average of C_{12}, C_{13}, and C_{23}; and E and B are calculated respectively by

$$E = \frac{(\overline{C}_{11} - L)(\overline{C}_{11} + 2L)}{\overline{C}_{11} + L}, \quad B = \frac{\overline{C}_{11} + 2L}{3}, \quad (14)$$

Table 3
Young's modulus, bulk modulus, shear modulus, and Lamé constant of unirradiated and irradiated fused silica cells

Cell#	E (GPa)	B (GPa)	G (GPa)	L (GPa)
1[a]	67.2 ± 6.4	30.3 ± 4.3	30.2 ± 2.8	10.3 ± 4.2
2[b]	74.8 ± 9.0	43.0 ± 6.0	31.3 ± 4.9	22.3 ± 6.5
3[c]	95.9 ± 14.2	57.5 ± 4.7	35.9 ± 3.5	31.2 ± 5.2
Experiment[d]	72.7	35.4	31.4	14.5[e]

[a] Unirradiated cell.
[b] $F_1 = 0.053\,\text{J/cm}^2$, $\tau = 50\,\text{ps}$, $D = 8.4\%$.
[c] $F_1 = 0.106\,\text{J/cm}^2$, $\tau = 100\,\text{ps}$, $D = 14.8\%$.
[d] Ref. [45].
[e] Calculated from E and G in Ref. [45] according to $L = G(E - 2G)/(3G - E)$.

where $\overline{C}_{11}$ is the average of C_{11}, C_{22}, and C_{33}, and the subscripts of C_{ij} follow Voigt's notation. The corresponding experimental data are also included in Table 3 to show that the simulated elastic constants of unirradiated fused silica are in good agreement with the experimental ones. We observe that Young's modulus, bulk modulus, and Lamé constant of fused silica increase rapidly after laser irradiation, while the shear modulus increases only slightly (18.8% compared to 42.7% in E, 89.8% in B, and 203.2% in L for Cell#3). In the experimental work of Meade and Jeanloz [43], the bulk modulus of silica glass was found to increase with applied hydrostatic pressure. Another MD study also reported the increase of E, G, and B with the density of nanophase silica glass [44], in which simulation cells containing more than one million atoms were studied without applying periodic boundary conditions and the densities of amorphous silica ranged from 1.67 to $2.03\,\text{g/cm}^3$.

5. Conclusions

We have performed classical molecular dynamics simulations to study UV-laser-induced densification in fused silica. With a model of energy transfer for laser irradiation, densification is observed in fused silica simulation cells. Relationships between absorbed laser fluence and induced densification at 193 nm are studied for laser fluences of up to $0.16\,\text{J/cm}^2$ and two laser durations (50 ps and 100 ps). For $\tau = 50\,\text{ps}$, densification is found to decrease mildly beyond $F_1 \sim 0.08\,\text{J/cm}^2$. In the case of $\tau = 100\,\text{ps}$, densification increases monotonically with absorbed laser fluence. Therefore we propose that a different laser pulse duration produces a different form of the relationship between laser fluence and densification. In both cases, the induced densification is of the order of 5%, which is in reasonable agreement with another MD study and with high-fluence laser irradiation experiments on fused silica.

Microstructural properties and elastic constants of fused silica are investigated to study to effects of laser irradiation. By comparing these properties of unirradiated cell and irradiated cells, we find that the length of the Si–O bond is little affected by laser irradiation, but those of O–O and Si–Si become shorter; over-coordinated Si atoms and O atoms appear after laser irradiation and their numbers increase with increasing density; the average bond angles of ∠O–Si–O and ∠Si–O–Si decrease with density; the number of 6-member rings decreases after irradiation with the others increasing, and both 6- and 7-member rings become dominant at a densification of 14.8%; Young's modulus, bulk modulus, and Lamé constant increase rapidly with density while the shear modulus increases at a much lower rate.

Acknowledgments

This work was supported by the US Department of Energy Office of Inertial Confinement Fusion under Cooperative Agreement No. DE-FC03-92SF19460, the University of Rochester, and the New York State Energy Research and Development Authority. The support of DOE does not constitute an endorsement by DOE of the views expressed in this article. One of the authors (L.Z.) thanks R.C.L. Vink for providing the initial simulation cell of fused silica and the Laboratory for Laser Energetics for a Horton Fellowship.

References

[1] T.P. Seward III, C. Smith, N.F. Borrelli, D.C. Allan, J. Non-Cryst. Solids 222 (1997) 407.
[2] D.H. Levy, K.K. Gleason, J. Appl. Phys. 73 (1993) 2809.
[3] W. Primak, L.H. Fuchs, P. Day, Phys. Rev. 92 (1953) 1064.
[4] W. Primak, R. Kampwirth, J. Appl. Phys. 39 (1968) 5651.
[5] C. Fiori, R.A.B. Devine, Phys. Rev. B 33 (1986) 2972.
[6] M. Rothschild, D.J. Ehrlich, D.C. Shaver, Appl. Phys. Lett. 55 (1989) 1276.
[7] R.E. Schenker, W.G. Oldham, J. Appl. Phys. 82 (1997) 1065.
[8] F. Piao, W.G. Oldham, E.E. Haller, J. Vac. Sci. Technol. B 16 (1998) 3419.
[9] V. Liberman, M. Rothschild, J.H.C. Sedlacek, R.S. Uttaro, A. Grenville, J. Non-Cryst. Solids 244 (1999) 159.
[10] C.K. Van Peski, R. Morton, Z. Bor, J. Non-Cryst. Solids 265 (2000) 285.
[11] B. Kühn, B. Uebbing, M. Stamminger, I. Radosevic, S. Kaiser, J. Non-Cryst. Solids 330 (2003) 23.
[12] L.V. Woodcock, C.A. Angell, P. Cheeseman, J. Chem. Phys. 65 (1976) 1565.
[13] P. Vashishta, R.K. Kalia, J.P. Rino, I. Ebbsjö, Phys. Rev. B 41 (1990) 12197.
[14] R.G. Della Valle, H.C. Andersen, J. Chem. Phys. 97 (1992) 2682.
[15] K. Vollmayr, W. Kob, K. Binder, Phys. Rev. B 54 (1996) 15808.
[16] J.S. Tse, D.D. Klug, Y.L. Page, Phys. Rev. B 46 (1992) 5933.
[17] W. Jin, R.K. Kalia, P. Vashishta, Phys. Rev. B 50 (1994) 118.
[18] K. Trachenko, M.T. Dove, J. Phys.: Condens. Matter 14 (2002) 7449.

[19] A. Kubota, M.-J. Caturla, J.S. Stölken, M.D. Feit, Opt. Express 8 (2001) 611.
[20] A. Wootton, B. Thomas, P. Harrowell, J. Chem. Phys. 115 (2001) 3336.
[21] K. Refson, Moldy User's Manual, Department of Earth Sciences, Oxford, UK, revision: 2.25.2.6 for release 2.16, 2001.
[22] M. Parrinello, A. Rahman, Phys. Rev. Lett. 45 (1980) 1196.
[23] J.R. Ray, A. Rahman, J. Chem. Phys. 80 (1984) 4423.
[24] S. Nosé, J. Chem. Phys. 81 (1984) 511.
[25] J.V. Lill, Comput. Phys. Commun. 79 (1994) 219.
[26] B.W.H. van Beest, G.J. Kramer, R.A. van Santen, Phys. Rev. Lett. 64 (1990) 1955.
[27] I. Saika-Voivod, F. Sciortino, P.H. Poole, Phys. Rev. E 63 (2000) 011202-1.
[28] U. Essmann, L. Perera, M.L. Berkowitz, T. Darden, H. Lee, L.G. Pedersen, J. Chem. Phys. 103 (1995) 8577.
[29] D.C. Rapaport, The Art of Molecular Dynamics Simulation, Cambridge University, Cambridge, UK, 1995.
[30] M.P. Allen, D.J. Tildesley, Computer Simulation of Liquids, Clarendon, Oxford, UK, 1987.
[31] P.A. Atanasov, N.N. Nedialkov, S.E. Imamova, A. Ruf, H. Hügel, F. Dausinger, P. Berger, Appl. Surf. Sci. 186 (2002) 369.
[32] R.L.C. Vink, G.T. Barkema, Phys. Rev. B 67 (2003) 245201-1.
[33] F. Wooten, K. Winer, D. Weaire, Phys. Rev. Lett. 54 (1985) 1392.
[34] V. Liberman, M. Rothschild, J.H.C. Sedlacek, R.S. Uttaro, A.K. Bates, C. Van Peski, Proc. SPIE 3578 (1998) 2.
[35] J. Wong, D.L. Haupt, J.H. Kinney, J. Ferriera, I.D. Hutcheon, S.G. Demos, M.R. Kozlowski, Proc. SPIE 4347 (2001) 466.
[36] G. Gutiérrez, Phys. Rev. B 65 (2002) 104202-1.
[37] Y. Inamura, M. Arai, M. Nakamura, T. Otomo, N. Kitamura, S.M. Bennington, A.C. Hannon, U. Buchenau, J. Non-Cryst. Solids 293–295 (2001) 389.
[38] C. Meade, R.J. Hemley, H.K. Mao, Phys. Rev. Lett. 69 (1992) 1387.
[39] K. Awazu, H. Kawazoe, J. Appl. Phys. 94 (2003) 6243.
[40] X. Yuan, A.N. Cormack, Comput. Mater. Sci. 24 (2002) 343.
[41] A. Pasquarello, R. Car, Phys. Rev. Lett. 80 (1998) 5145.
[42] J.R. Ray, M.C. Moody, A. Rahman, Phys. Rev. B 32 (1985) 733.
[43] C. Meade, R. Jeanloz, Phys. Rev. B 35 (1987) 236.
[44] T. Campbell, R.K. Kalia, A. Nakano, F. Shimojo, K. Tsuruta, P. Vashishta, S. Ogata, Phys. Rev. Lett. 82 (1999) 4018.
[45] Product sheet for HPFS® 7980 standard grade, Corning, NY. http://www.corning.com.